SANDIA REPORT
SAND2009-3080
Unlimited Release
Printed April 2009

Micro-System Inertial Sensing Technology Overview

James J. Allen

Prepared by
Sandia National Laboratories
Albuquerque, New Mexico 87185 and Livermore, California 94550

Sandia is a multiprogram laboratory operated by Sandia Corporation,
a Lockheed Martin Company, for the United States Department of Energy's
National Nuclear Security Administration under Contract DE-AC04-94AL85000.

Issued by Sandia National Laboratories, operated for the United States Department of Energy by Sandia Corporation.

Available to DOE and DOE contractors from
U.S. Department of Energy
Office of Scientific and Technical Information
P.O. Box 62
Oak Ridge, TN 37831

Telephone: (865) 576-8401
Facsimile: (865) 576-5728
E-Mail: reports@adonis.osti.gov
Online ordering: http://www.osti.gov/bridge

Available to the public from
U.S. Department of Commerce
National Technical Information Service
5285 Port Royal Rd.
Springfield, VA 22161

Telephone: (800) 553-6847
Facsimile: (703) 605-6900
E-Mail: orders@ntis.fedworld.gov
Online order: http://www.ntis.gov/help/ordermethods.asp?loc=7-4-0#online

SAND2009-3080
Unlimited Release
Printed February 2009

Micro-System Inertial Sensing Technology Overview

James J. Allen[1]
Intelligent Systems Controls Department
Sandia National Laboratories
P.O. Box 5800
Albuquerque, New Mexico 87185-MS0783

Abstract

The purpose of this report is to provide an overview of Micro-System technology as it applies to inertial sensing. Transduction methods are reviewed with capacitance and piezoresistive being the most often used in COTS Micro-electro-mechanical system (MEMS) inertial sensors. Optical transduction is the most recent transduction method having significant impact on improving sensor resolution. A few other methods are motioned which are in a R&D status to hopefully allow MEMS inertial sensors to become viable as a navigation grade sensor. The accelerometer, gyroscope and gravity gradiometer are the type of inertial sensors which are reviewed in this report. Their method of operation and a sampling of COTS sensors and grade are reviewed as well.

[1] Member of the "MEMS Technologies Department" at the time of this work.

ACKNOWLEDGMENTS

Sandia is a multi-program laboratory operated by Sandia Corporation, a Lockheed Martin Company, for the United States Department of Energy under contract DE-AC04-94AL85000.

CONTENTS

FIGURES

TABLES

1. INTRODUCTION

The first inertial navigation systems were used in the German V1 and V2 weapons of World War II. This was later developed for ICBM and Naval Ship Inertial Navigation Systems (SINS) at the Redstone Arsenal in Huntsville, Alabama and at Draper Laboratories in Massachusetts, respectively.

The inertial properties of matter or light are utilized in gyroscopes and accelerometers to provide estimates of heading and velocity to perform a "dead reckoning" style of navigation. An inertial measurement unit (IMU) would contain 3 axes of gyroscopes and 3 axes of acceleration measurement instruments to provide the information for navigation in 3 dimensions. Many modern IMU implementations may also contain a Global Positioning System (GPS) instrument to supplement the inertial instruments data to aid the navigation algorithms in obtaining the navigation estimates.

Table 1 shows representative accelerometer and gyroscope performance requirements for the different performance grades of inertial sensing. There are military applications that span all of these performance grades from strategic (e.g. ICBM navigation) to tactical (e.g. short time of flight navigation of artillery shells) to instrument (e.g. automobile impact and anti-roll sensors).

Table 1. IMU Performance Grade versus Inertial Sensor Bias Stability Requirements.

Performance Grade	Accelerometer Bias Stability	Gyroscope Bias Stability
Strategic	< 1 μg	<0.0001 °/hr
Navigation	10 – 50 μg	0.001 – 0.01 °/hr
Tactical	0.1 – 1 mg	1 – 10 °/hr
Instrumentation	10 – 100 mg	30 – 100 °/hr

Microelectromechanical system (MEMS) technology greatly enables military applications by the ability to produce small, low power, rugged sensors. However, the miniaturization of sensors is frequently a double edged sword due to competing physical effects where reduction in size can enhance one aspect but degrade another. For example, the poor relative tolerances of MEMS manufacturing compared to macro-scale manufacturing are a contributor to the greater bias of MEMS inertial sensors. MEMS inertial sensors currently have the ability to address *instrument grade* (e.g. *Analog Devices* – ADXL and ADRS series, *Endevco*) applications. The Honeywell IMU initially developed by DRAPER Laboratories has recently been able to meet *tactical grade* requirements. *Bias stability is one of the dominant factors which must be reduced* to enable MEMS inertial sensors to meet *navigation grade* performance requirements.

While the discussion of the previous paragraph refers specifically to the state of the art of existing commercially available MEMS sensors, the research to provide sensors of increasing accuracy is advancing. This research is being funded by Defense Advanced Research Projects Agency (DARPA), Office of Naval Research (ONR) and the Sandia Laboratory Directed Research and Development (LDRD) program. Sandia is participating in several DARPA and ONR programs to improve MEMS inertial sensor capability.

The following sections will discuss the various transduction methods utilized in existing MEMS inertial sensors as well as the advanced method being researched to provide new avenues of improved performance.

2. TRANSDUCTION METHODS

2.1 Capacitance Sensing

Electrostatic capacitance sensing is a frequently used transduction method for MEMS devices. MEMS fabrication techniques can readily produce parallel plate or inter-digitated comb finger capacitors in a MEMS device that can move as a result of a physical variable (acceleration, pressure) excitation. The relative motion of the plates can be in any direction (vertical, horizontal).

The size of the capacitors utilized in MEMS devices are small, generally a fraction of a pico-Farad. The variation of the nominal capacitance that is to be sensed to provide the dynamic signal of interest is in the femto-Farad range or less. There are also undesirable stray capacitances called *parasitic capacitances* which can interfere with capacitance sensing. These parasitic capacitances are between the sense lines, combs or plates and surrounding structures which provide erroneous signals not related to the actual physical measurement. The typical methods that are utilized to minimize parasitic capacitances involve packaging or fabrication methods which minimize distances between the portions of the accelerometer or gyroscope that are to be capacitatively sensed and the first stage of electronic amplification. This can be accomplished by either flip chip bonding the MEMS and electronic die together or utilizing an integrated MEMS (IMEMS) fabrication process.

There are three approaches for the implementation of an Integrated MEMS (IMEMS) fabrication processes which can produce the electronics and the sense structure on a single chip. The strategies are Microelectronics First, Interleave the Microelectronics and MEMS fabrication, and MEMS fabrication first which are illustrated in Figure 1.

Capacitive sensing is utilized in successful commercial MEMS sensors which address both the tactical and instrument grades (i.e. Honeywell, Analog devices respectively)

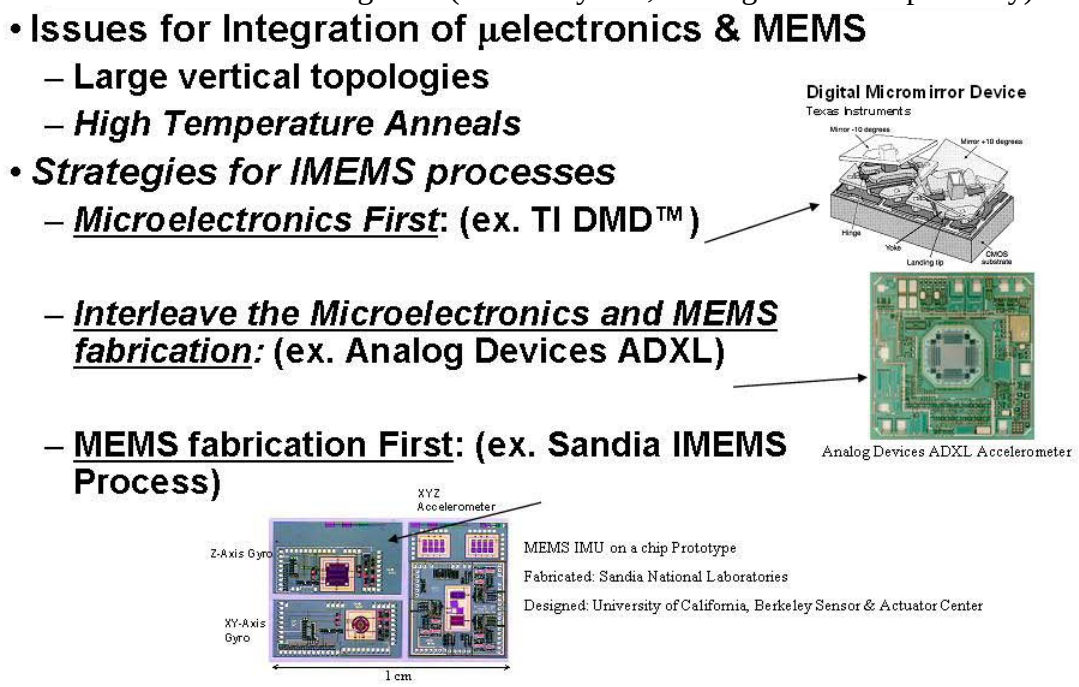

Figure 1. Issues and Strategies for Implementation of IMEMS Processes.

2.2 Piezoresistive Sensing

Piezoresistivity is a widely utilized phenomenon for MEMS sensors. The piezoresistive effect was first discovered by Lord Kelvin in 1856 when he reported that certain metallic (iron, copper) conductors under mechanical strain exhibited a corresponding change in electrical resistance. This is the basic operating principle for metal and foil strain gauges which have been used for engineering measurements for many years. The piezoresistive effect in single crystal silicon and germanium was first reported in 1954. The discovery of the piezoresistive effect in silicon had significant impact in the development of MEMS for the following reasons.

- Integration with MEMS devices and micro electronics is possible due to material compatibility
- Integration of the piezoresistive material and the MEMS device allow good transmission of strain without hysteresis or creep.
- The piezoresistive effect in silicon is over an order of magnitude greater than metals.
- MEMS fabrication processes allow good matching of resistors utilized in the Wheatstone bride sensing circuits.

The sense circuitry is typically a Wheatstone bridge. Piezoresistive Sensing for measurement grade bulk micromachined accelerometers is widely used for commercial accelerometers.

2.3 Electron Tunneling

There exists an extensive literature base on *tunneling tip* methods of transduction. The method was initially used in the scanning tunneling microscope [1] (STM) which has been used in material science research such as the study of atomic scale surface structure. This method of transduction has also been used for infrared (IR) [2], magnetometer [3], and accelerometer sensors [4]. Electron tunneling can provide an extremely sensitive method of position transduction.

Electron tunneling is a phenomenon in which a current is passed across a narrow gap, Figure 2. Classically, a gap of finite size would pose a barrier to current flow. However, for sufficiently small gaps ($\sim 10\,\text{Å}$) the probabilistic nature of quantum mechanics becomes apparent. In quantum mechanics when a particle comes to a barrier that it doesn't have enough energy to penetrate, the wave function dies off exponentially. However, if the gap is small enough, the wave function will predict a significant probability of finding the particle on the other side of the gap. Therefore, if the gap is small enough, a tunneling current will exist even though there is a break in the circuit.

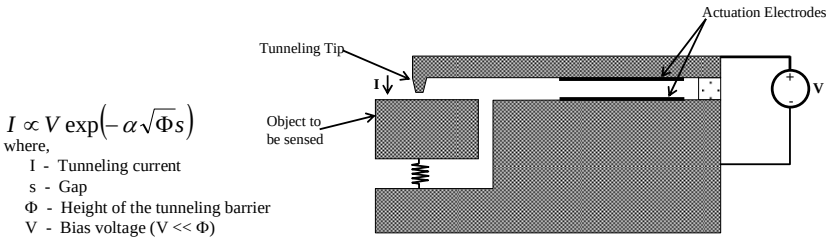

Figure 8.34 Electron Tunneling Transduction Schematic

* Quantum Mechanic effect
* The tip and opposing surface are metalized.
* Gap of ~ 10 nm, controlled by feedback.
* Tip geometry not crucial (1-5μm radius of curvature)
* Extremely sensitive to small displacements

Figure 2. Schematic of an electron tunneling tip transducer.

The tunneling tip and opposing surface must be metalized with a thin layer of metal such as 100 Å of gold which is adequate for this purpose. The tunnel effect is not extremely sensitive to tip geometry. One reported tunneling tip was a 50μm pyramid with a 1-5μm radius of curvature and even a 5μm mesa will suffice. This makes the fabrication of the tunneling tip more tractable.

Since the tunneling tip is so close to the surface of a moving mass or membrane to be measured, the gap must be controlled by feedback during operation. This can be accomplished by measuring the tunneling current, and applying correction signals an actuator to control either the tunneling tip or the moving mass or membrane. Since the tunneling tip is small it can be controlled with minimal effort.

This method of transduction has been demonstrated in R&D prototypes, there are no commercial devices available.

2.4 Optical Sensing

Until recently, the most promising technique for a highly-sensitive displacement sensor has been the tunneling transducer. Using such a transducer, Liu and Kenny have demonstrated an accelerometer with sensitivity approaching 20 ng/√Hz in a 5 Hz–1.5 kHz band [5]. These devices, however, have a relatively limited dynamic range and require extensive control architectures that add cost and increase the noise floor at low frequencies. The broad use of MEMS inertial sensors is, in great part, because of their low cost and inherently small size and weight. However, the limiting noise factors become significantly worse as the size decreases. *Optical detection techniques offer ways of overcoming some of these limitations.* High-sensitivity micromachined accelerometers using optical interferometer techniques have been demonstrated by Waters and Aklufi (2002) [6] and Loh, et al (2002) [7], but with less sensitivity than the device based on tunneling transducers.

The Advanced MEMS Technologies Department at Sandia National Laboratories (SNL) has built some of the most sensitive displacement sensors on record based on a grating - reflector style optical transducer (B.E.N. Keeler et al, 2004 [8], Hall et al, 2006, [9]). Displacement sensitivity of 12 fm/√Hz with a optical nano-grating sensor and 20 fm/√Hz with a diffraction grating sensor have been demonstrated. SNL has shown optical microphones and prototype

accelerometers based on the diffraction grating technique (Hall et al, 2008, [10]). A prototype accelerometer with thermal noise floor of 17 ng/√Hz was also fabricated and tested, which utilized an optical nano-grating approach (Krishnamoorthy et al, 2007 [11], Krishnamoorthy et al, 2008 [12]). *Optical sensing techniques do not suffer from scaling to very small sizes and the ultimate resolution and dynamic range that can be achieved is superior to other techniques.*

2.5 Atomic Interferometer

The fundamental concept of an atom interferometer and its use in inertial sensors has been described in the literature [13]. The wave-like nature of atoms is used to construct an atom interferometer analogous to laser interferometers.

An approach to realize an atom interferometer utilizes light pulses to split and recombine the atom beams which are required functions for an interferometer. When an atom absorbs or emits a photon, its momentum changes. The implementation of an atomic interferometer starts with a laser pulse that put the atom in an equal superposition of the ground and excited states. The excited state of the atom changes its momentum due to photon absorption the ground state remains unchanged, which accomplishes the atom wave beam splitting. Similarly other laser pulses can redirect and recombine the atom beams to form a Mach-Zehnder type interferometer, Figure 3.

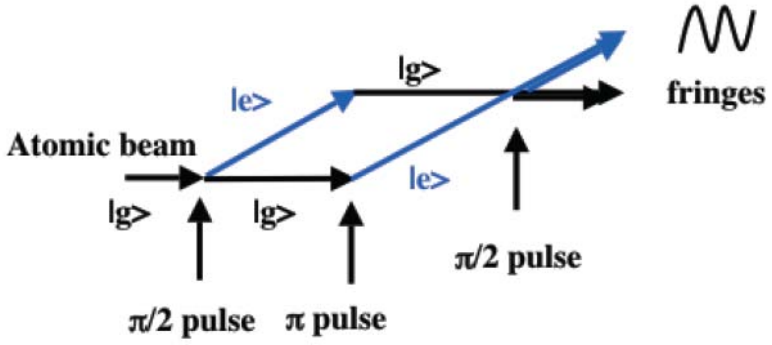

Figure 3. Illustration of a Mach-Zehnder atom Interferometer with light pulsed as atom wave optic.

The interferometer read out is accomplished by monitoring the relative populations of the two states of the recombined atoms via laser-induced fluorescence. Knowing the laser wave number k, and the interrogation time T, the gravity acceleration g can be determined by the equation 1. Atomic interferometers hold the promise of unprecedented sensitivity. For example reference 13 using the known properties of Cesium (Cs) atoms, a reasonable interrogation time and signal to noise of the fluorescence read out predicted a sensitivity of approximately 10^{-10} g.

1) $$\Delta\phi = kgT^2$$

Atomic interferometers are currently under research and development at several laboratories including Sandia National Laboratories. The challenges of realizing an instrument such as this include the Alkali Metal atom sources, vacuum packaging, lasers, laser cooling, etc. There are currently no commercial sources for an atomic interferometer instrument.

2.6 Nuclear Magnetic Resonance

The principal elements of a Nuclear Magnetic Resonance (NMR) sensor are a light source, an NMR cell, photo detector, magnetic shields and a set of magnetic field coils. The

NMR cell is mounted within a set of magnetic shields to attenuate external magnetic fields to acceptably low levels. Magnetic field coils are used to apply a very uniform magnetic field to the NMR cell. Both a steady field and an AC field are applied along the sensitive axis of the device, and an AC field is applied along one of the transverse axes. The NMR cell contains an alkali metal vapor (e.g. Rb, K, Cs) together with two isotopes of one or more noble gases (e.g. ^{129}Xe, ^{131}Xe, ^{83}Kr). A buffer gas such as He may also be contained in the cell. The cell is illuminated by a beam of circularly polarized light which optically aligns the magnetic moments of the alkali metal vapor, Figure 4. Alignment nuclear magnetic moments of the noble gas components of the cell are achieved by collisions with the optically aligned alkali metal magnetic moments (e.g. Rb or Cs). Detection of precessing nuclear moments can be sensed by a magnetometer.

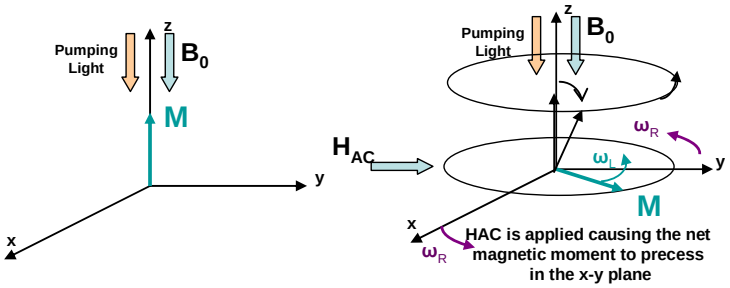

a) Pump light aligns spins and a magnetic field causes moments to precess at a known frequency

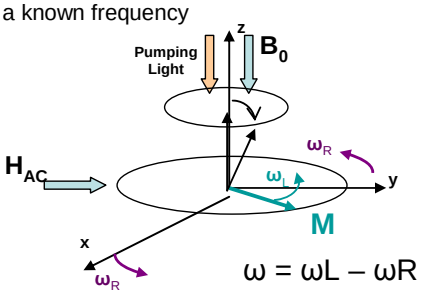

b) Inertial rotation of the gyro about the precession axis shifts the precession frequency by a detectable frequency and provides an accurate measure of inertial rate

Figure 4. NMR Gyroscope Concept of Operation

Litton developed a large table top size NMR gyro in 1968-1982 with a demonstrated performance of 0.01 deg/hr [14]. DARPA is currently funding various approaches to achieving a small (1cc), low power (5mW), navigation grade gyroscope as part of the NGIMG program. Sandia is working with external partners Northrop Grumman and the California Institute of Technology to execute this multi-phase program. This team's approach employs the principles of Nuclear Magnetic Resonance to achieve gyro operation. Microfabrication techniques provide a path to implementing a smaller NMR Gyro today. This effort is currently in phase 2 of the program.

3. TYPES OF INERTIAL SENSORS

Accelerometers and gyroscopes are inertial sensors which measure acceleration and rotation rate respectively. For purposes of navigation these two types of sensors provide direction and heading information. The performance grades of these types of sensors are presented in Table 1. This table presents the bias stability range for the four performance grades. The performance varies from strategic grade inertial instruments which are used on strategic missiles, and submarines, to instrument grade instruments which are used in automotive and consumer applications. Currently, MEMS inertial sensors are commercially available in the tactical and instrument grade inertial sensors.

3.1 Accelerometer

Accelerometers are one of the most frequently utilized physical sensors for detecting and measurement of motion. Accelerometers have found application ranging from measurement and control to inertial navigation. MEMS implementations of accelerometers have found a large commercial market in automotive airbag deployment systems. The basic configuration of an accelerometer is the same for all of these applications.

Figure 5 schematically depicts the basic elements of an accelerometer. This device consists of a mass (M) suspended by a suspension of stiffness (K) within a case or housing. The mass will have damping force acting on the mass due to the internal environment which causes energy to be lost from the mass.

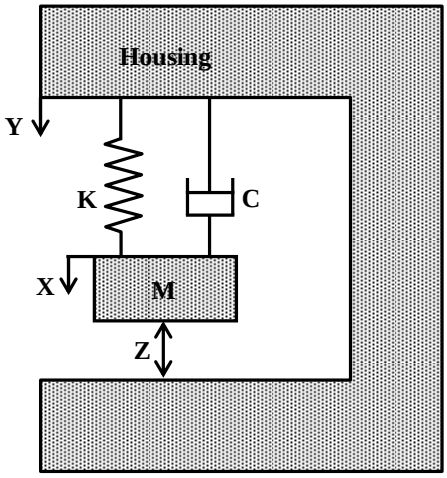

Figure 5. Schematic depiction of an accelerometer.

$$M\ddot{Z} + C\dot{Z} + KZ = M\ddot{Y} \qquad \textbf{2)}$$

$$\ddot{Z} + 2\xi\omega_n\dot{Z} + \omega_n^2 Z = \ddot{Y}$$

The equation 2 is a second order differential equation which describes the motion of the accelerometer. The acceleration $\ddot{Y}$ is applied to external housing of the accelerometer. The motion that will be transduced as a measure of the housing acceleration is the acceleration of the suspended mass *relative* to the housing, $\ddot{Z}$. Any of the previously mentioned methods of transduction can be used in the accelerometer.

A second order differential equation will have a resonance at the system natural frequency, ω_n. Resonance is a condition where the spring forces balance the inertia forces and the damping force control the amplitude. The damping ratio, ζ is a measure of the system damping. With no damping the amplitude of the system would theoretically become infinite. The response varies from oscillatory for $\zeta < 1$ to non-oscillatory for $\zeta \geq 1$.

The design of an accelerometer is very dependent upon the system damping. The amount of damping will determine the dynamic response and the Brownian noise and hence the noise floor of the sensor.

Macro size accelerometers are designed to have a damping ratio of $\zeta \cong 0.7$. This type of system will have a fast response with very small overshoot. The accelerometer needs to sense signals which contain a combination of many frequencies. Two metrics which are important for accelerometer design are *amplitude distortion* and *phase distortion*. To prevent amplitude distortion the accelerometer transfer function must amplify the signals of different frequencies equally. This means the magnitude of the frequency response must be flat in the operating range which occurs in the low frequency range of the sensor [15]. For no phase distortion the phase of the harmonic components of the signal must increase linearly with frequency. This will shift the harmonic components in time equally. A damping ratio of $\zeta \cong 0.7$ almost perfectly eliminates phase distortion, and restricting the operating range to approximately $0 < \omega/\omega_n \leq 0.1$ also minimize amplitude distortion. For most MEMS accelerometer designs the natural frequency of the inertial mass – suspension system is at least an order of magnitude higher than the highest frequency signal to be sensed.

The mechanical sensitivity of an accelerometer, S_M, is the relationship between the relative deflection of the inertial mass and case, Z, and the input acceleration, $\ddot{Y}$. Since the operating range of the accelerometer is at low frequency, where $\omega \approx 0$, the dynamic forces are negligible, and the mechanical sensitivity, S_M, of an accelerometer is as shown in the equation 3.

3) $$S_M = \frac{M}{K} = \frac{1}{\omega_n^2}$$

The accelerometer described thus far is an *open-loop sensor* which consists of the inertial mass- suspension system, position sensing, and amplification - signal conditioning elements. For an open loop accelerometer the greater the acceleration $\ddot{Y}$ input the greater the relative displacement, Z which will be transduced into an electrical signal. Linearity is an important sensor quality because of calibration and signal conditioning issues. However, some of the transduction means such as capacitance sensing are non-linear with increasing displacement. This can be mitigated by limiting the acceleration input range of the sensor, but this also has the adverse effect of limiting the sensor dynamic range. Generally an open loop accelerometer is satisfactory for applications where the dynamic range is less than 1000:1 and where the scale factor error can be 0.1% or greater. This is generally the case for instrument grade accelerometers; however, for accelerometers used in inertial navigation this is not sufficient.

An alternative approach is to maintain the inertial mass in the un-deflected or zero position during acceleration. This will require a control loop with a force actuator to maintain the inertial mass position. A *closed loop sensor* involves some additional items compared to an open loop sensor. The closed loop accelerometer will need an actuator to apply force on the inertial mass to maintain its position, and a control compensator to maintain the closed loop stability of the system.

There are a number of tradeoffs associated with an open loop versus closed loop or analog versus digital implementation of an accelerometer. The sensitivity and bandwidth of the open loop accelerometer are both related to the natural frequency, ω_n, of the suspension. The closed loop accelerometer implementation can make the sensitivity – bandwidth tradeoff somewhat independently and reduce the impact of nonlinearities (e.g. electrostatics) on the sensor. However, a closed loop accelerometer implementation will be limited by the capacity of the force actuation to balance the inertial mass for high input accelerations. Therefore most accelerometers to be used in high g shock measurements are open loop devices.

3.1.1 MEMS Accelerometer COTS Suppliers and Grades

Measurement and tactical grade MEMS accelerometers are commercially available with a variety of packaging types and interface options. The measurement grade devices are targeted primarily at large volume applications such as automotive and motion/orientation sensing markets. Since the volume is high the cost per device can be low, but the ability to specialize the package and interface is limited without significant additional cost. The tactical navigation gyroscope applications are targeted mainly for a smaller military market, thus the cost can be significantly higher. Table 2 is an attempt to summarize companies who can supply these COTS parts.

Table 2. COTS MEMS Accelerometer Grades and Suppliers.

Sensor Technology	**Sensitivity (Bias Stability)**	**Power**	**Cost**	**Supplier**	**Product Series**
Measurement Grade	10-100 mg	< 1 mW	~ $5 to several $100 ea	www.analog.com	ADXL
				www.xbow.com	TG
				www.colibrys.com	Si-Flex
				www.kionix.com	KX
				www.endevco.com	
				www.isense.com	InertiaCube2 (note 2)
				www.semiconductors.bosch.de	SMB
				www.memsense.com	
Tactical Grade	~ 1 mg	100mW – 500mW	~$1K/ea	www.honeywell.com	QA
				www.northropgrumman.com	LN (note 1)

Note:

1. LN series is an IMU which contains an accelerometer
2. InertiaCube2 is an orientation sensor (yaw, pitch, roll)

3.2 Gyroscope

A gyroscope is an inertial instrument which is capable of sensing rotation. A gyroscope can be implemented in a number of ways. The first gyroscope invented by Leon Foucault in 1852 was based on the angular momentum of a spinning wheel. Since that time several

alternative methods have been developed to meet the applications needs, particularly in navigation.

3.2.1 Spinning Mass Gyroscope

The spinning mass gyroscope is based on the angular momentum of a rotating body. The angular momentum, H is the product of the mass moment of inertia, I and the angular velocity, ω, of the wheel, equation 4. Due to Newton's Law's of Motion, the angular momentum of a body will remain unchanged unless acted on by a torque, T, equation 5 . If a torque is applied in the same axis as the angular velocity, the effect is to accelerate/decelerate the rotating body, which is denoted by the first term of equation 5. However, if the torque is applied orthogonal to the spin axis the rotating body will precess, Ω, denoted by the second term of equation 5. These effects illustrated in the cross product in the second term generates the interesting gyroscopic effects (i.e. Ω, H, and T are related by the right hand rule). Precession or the moments generated by precession is the effect utilized by this form of gyroscope as a measure of angular rate.

The spinning wheel gyroscope is used to implement a class of high performance gyroscopes for inertial navigation as well as other lower performance applications. The fabrication of this type of gyroscope requires precision bearings, machining, drive motors and electronics which makes them very costly. However, in the 1950's inertial navigation for missiles, aircraft, submarines came to rely on this type of gyroscope.

4) $$H = I\omega$$

5) $$T = \frac{dH}{dt} + \Omega \times H$$

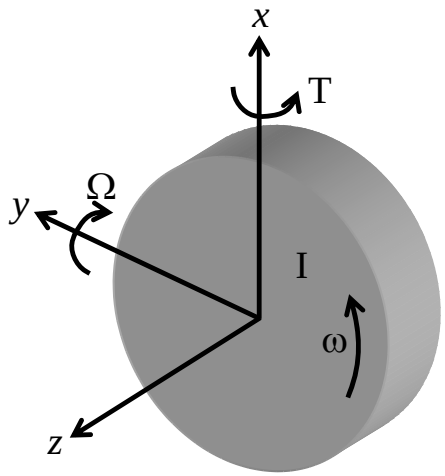

Figure 6 Precession of a rotating body.

In the 1980's and 1990's when MEMS technology was reaching the stage of maturity sufficient for application to gyroscopic sensing several avenues were pursued. The development of a MEMS spinning mass gyroscope was initially inhibited due to the lack of low friction bearings and the significant stiction and adhesion forces at the micro-scale. However, promising research on the development of an electrostatic levitated spinning mass MEMS gyroscope is proceeding [16,17]. This is an ambitious approach due to the necessity of closed loop control to

stabilize the levitation, in addition to driving the spinning mass and sensing its deflections due to precession. The DARPA Navigation Grade Integrated Micro Gyroscopes (NGIMG) program has funded Archangel System Inc. [18] to develop a MEMS spinning mass gyroscope. The development of a MEMS rotating mass gyroscope is currently in the research stages with no commercial products available.

3.2.2 Optical Gyroscope

Optical rotation rate sensors based upon the *Sagnac effect* have also been developed [19]. The Sagnac effect was discovered by Georges Sagnac in 1913 while performing a modification of the Michelson-Morley experiment. An optical gyroscope utilizing the Sagnac effect can be implemented with two counter-rotating light beams circulating around an optical path of radius, R, where the optical path itself is rotating with angular velocity, Ω, Figure 7. The Sagnac effect can be observed by the time difference, Δt, between the clockwise and counterclockwise beams striking a detector which is in the optical path and rotating with the optical path. If the optical path is not rotating, the optical signal traveling in either direction will complete the path at the same time. However if the optical path is rotating clockwise as shown in Figure 7.b, the optical signal traveling in the same direction as the rotation will have a slightly longer distance to travel than the optical signal traveling in the opposite direction. The tangential speed of the rotating optical path is v= ΩR. The initial separation of the start and end point of the optical signals are 2πR, or if we allow the signal to circulate N times around the path N2πR. The time difference in the arrival of the signals due to the Sagnac effect can be calculated as shown in equation 6, where c is the speed of light in the optical path medium. The Sagnac effect time interval is very small. For example, the measurement the Earth's rotation rate (i.e. 15°/hr) with a 1 Km long optical path will produce a Sagnac effect of only $\Delta t=3.3\times10^{-9}$ sec. A short time interval such as this can be resolved by phase shift effects of the optical signals.

6) $$\Delta t = N2\pi R\left(\frac{1}{c-v}-\frac{1}{c+v}\right)\approx\frac{\mathrm{N}4\pi R^2\Omega}{\mathrm{c}^2}$$

The basic configuration schematically described in

Figure 7, can be implemented with fiber optics with multiple turns (N) to increase path length and the Δt or phase shift measured as an indication of rotation rate, Ω. The Sagnac effect is the basis for a number of optical rotation rate sensors such as the Interferometric Fiber-Optic Gyro (IFOG). There are a number of macro size gyroscopes of this type which are commercially available.

In 1982 a micro-optical-gyro (MOG) concept utilizing MEMS and microelectronic fabrication techniques was patented, and initial development pursued by Northrup [20,21]. MOG's utilize waveguides etched into the substrate by MEMS etching techniques. This initial effort by Northrup to produce an MOG was discontinued. However, other organizations [22,23] are still pursuing this concept; but, this approach does not currently have a MOG commercial product available,

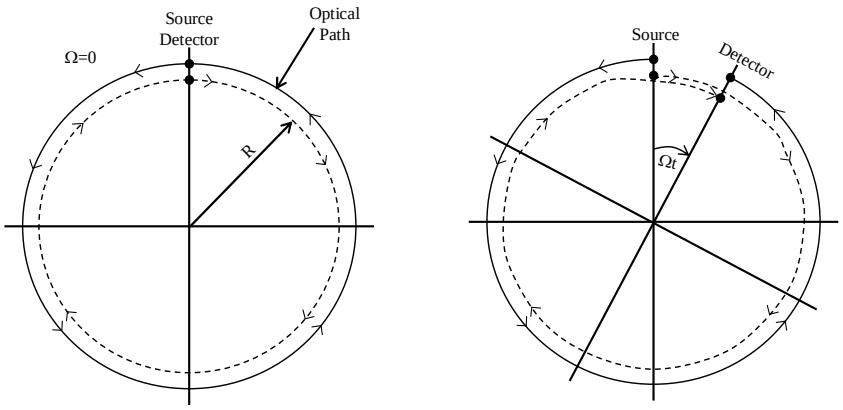

a. Optical path stationary

b. Optical path rotating with angular velocity Ω

Figure 7. Sagnac effect on two counter rotating beams of light.

3.2.3 Vibratory Gyroscope

Another approach for rotation rate sensing lies in the dynamics of vibrating mechanical systems. The fact that vibrating objects are sensitive to rotation has been known since 1890. The initial concept for an implementable *vibratory gyroscope* was based on the vibration of a metal tuning fork [24,25]. By the 1960's, engineers were seeking alternatives to the spinning mass gyroscope due to its size, fragility and expense. Subsequent technology developments enabled the realization of a functioning vibratory gyroscope [26-28]. The vibratory gyroscope was also later discovered to be the mechanism utilized by biological systems such as fly's ability to sense angular rotation [29].

Vibratory gyroscopes are based on sensing *Coriolis acceleration*, which is acceleration produced due to the changing direction in space of the velocity of the body relative to the moving system. For example, Figure 8, shows the Coriolis acceleration, $A_{Coriolis}$, produced on a body that is moving around an axis with a fixed angular velocity, Ω, and moving radially with a velocity, V as well. The Coriolis acceleration is defined by equation **7**. The detection of the deflection of an object due to Coriolis acceleration is the basis for a vibratory gyroscope.

7) $$A_{coriolis} = 2\Omega \times V$$

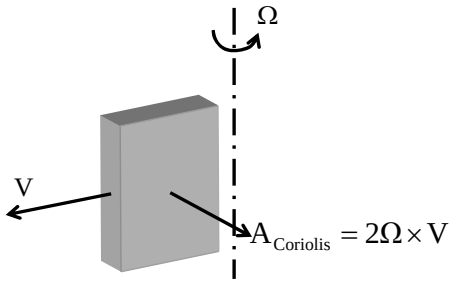

Figure 8 Coriolis acceleration on a moving body in a rotating system.

A vibratory gyroscope is comprised of a resonator which will oscillate a body along one axis and measure the orthogonal movement or force on the body due to Coriolis acceleration. Figure 9 is a schematic of a plate that is being driven along the x axis, the rotation rate to be measured, Ω is along the z axis and the Coriolis acceleration response is sensed along the y axis. Equations 8 and 9 are the equations of motion (force balance) for the body in the drive and sense

axes, respectively. These are a system of coupled second order equations which are coupled via to the Coriolis acceleration terms. The physical mechanism for a vibratory gyroscope is the transfer of energy from one resonator axis to another via the Coriolis acceleration coupling. The suspension for this device can have a unique natural frequency, ω_x, ω_y and a unique damping ratio for ζ_x, ζ_y each axis, equation 10. The relative positioning of the suspension natural frequencies is a gyroscope design decision. Frequently the sense direction natural frequency, ω_y, is approximately 10% less than the drive direction natural frequency, ω_x. This will provide a modest mechanical gain without significant bandwidth or phase shift reductions. The damping ratio of the mass in the x and y axes depend on the orientation of the mass relative to the substrate which will determine the damping mechanism involved (e.g. squeeze film versus lateral shear damping).

The implementation of the gyroscope will require the mass to be driven in the x axis by the force, F_x. For many MEMS designs the force, F_x, is electrostatic such as a interdigitated electrostatic comb drive. The drive amplitude, x must be maintained very accurately since any variation will directly contribute an error into the sense direction amplitude, equation 8 and the gyroscope output. For this reason the drive axis amplitude is controlled by an automatic gain control feedback loop.

Because the oscillatory drive portion of the gyroscope, equation 8 is fixed to a high degree of accuracy by the gain control loop, equation 9 governs the dynamics of the gyroscope response. Since the x axis (drive axis) is an oscillator the response of the y axis (sense axis) will also be oscillatory, equation 11. The Coriolis term which is the input to equation 9 is twice the product of the angular rate and the velocity of the x axis oscillator which produces a *modulated* signal. Therefore, the gyroscope output will need to be *demodulated* to extract the rotation rate signal.

The velocity, $\dot{x}$, of the drive signal which is the input to the Coriolis term of equation 9 is simple harmonic motion which will be zero at the extremes of motion of the driven mass and a maximum as the mass pass through the undeflected position. The mass x displacement and the Coriolis force which contains an x velocity term have a 90° phase difference; therefore the y displacement due to the Coriolis force will also have a 90° phase difference. These signals are said to be in *quadrature*. This will lead to an oval deflection path (symmetric about the x axis) of the mass shown in Figure 10.a when the gyroscope is subject to a constant rotation rate. With a zero rotation rate the mass deflection pattern will not deflect in the y direction and oscillate entirely along the x axis as shown in Figure 10.b.

However, if mass or stiffness imbalances exist in the system dynamics as indicated in equation 12, the mass deflection pattern will be as shown in Figure 10.c. These subtle imbalances in the vibration of the sense mass produces a deflection in the y direction known as *quadrature error* which contaminates the Coriolis signal which is the measure of rotation rate. The effects of quadrature error can be negated by a quadrature error cancellation [30,31] scheme which involves the used of electrostatic actuators with properly phased signals to cancel the imbalance, or by a synchronous detection methods which takes advantage of the quadrature relationship to extract the Coriolis signal.

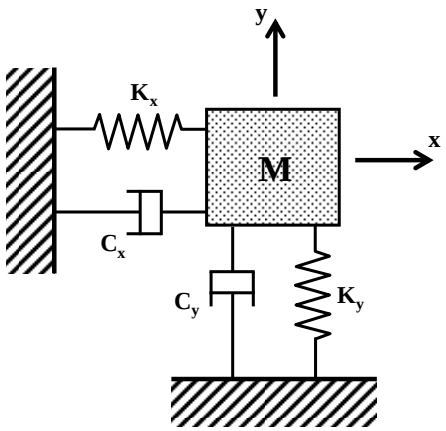

Figure 9. Single Mass Gyroscope Schematic

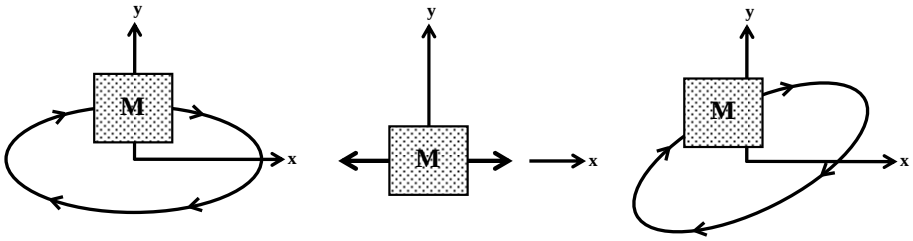

a. Ω≠0 deflection path b. Ω=0 deflection path c. Ω≠0 deflection path with quadrature error

Figure 10 Gyroscope mass deflection response due to Coriolis acceleration

8) $$\ddot{x} + 2\zeta_x\omega_x\dot{x} + \omega_x^2 x = \frac{1}{M}F_x - 2\Omega\dot{y}$$

9) $$\ddot{y} + 2\zeta_y\omega_y\dot{y} + \omega_y^2 y = 2\Omega\dot{x}$$

10) $$\omega_y = \sqrt{\frac{K_y}{M}} \qquad \omega_x = \sqrt{\frac{K_x}{M}}$$

11) $$x = Xe^{j\omega t} \qquad y = Ye^{j(\omega t+\varphi)}$$

12) $$\ddot{y} + \delta_M\ddot{x} + 2\zeta_y\omega_y\dot{y} + \omega_y^2 y + \delta_K x = 2\Omega\dot{x}$$

The first silicon integrated micromachined vibratory gyroscope was described by O'Connor and Shupe in 1981 [32]. In the ensuing years, development of a MEMS gyroscope was spurred by the lure of a low cost, mass producible instrument. There were efforts to produce single resonator gyroscopes schematically shown.

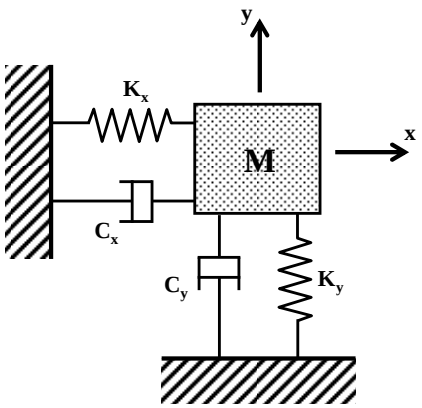

Figure 11. Single Mass Gyroscope Schematic

However, the one configuration that has been employed both for macro-scale and MEMS vibratory gyroscopes is the *tuning fork gyro* (TFG), Figure 12. The TFG consists of two masses that are driven in an anti-phase manner (i.e. both plates move outward and inward relative to the center axis). The rotational field will cause the plates to move perpendicular to the substrate in opposite directions. This configuration enables differential sensing which will allow common mode signals such as external accelerations to be rejected. The use of two masses vibrating in opposite phase also causes momenta to cancel locally and make the gyroscope less sensitive to mounting. The two masses may have coupled or separate suspensions.

MEMS TFG's have been successfully developed for commercial applications by Draper Laboratories [33,34] and Analog Device [35]. These are examples of tactical and instrument grade MEMS gyroscopes respectively. The applications for a gyroscope such as these include tactical grade navigation, platform stabilization, automobile skid control and stabilization, entertainment (i.e. Wii).

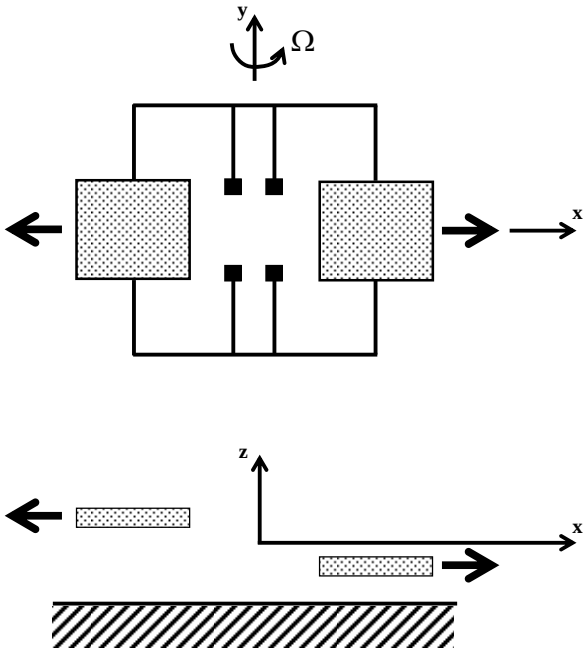

Figure 12. Tuning Fork Gyro (TFG) Schematic

3.2.4 MEMS Gyroscope Suppliers and Grades

Measurement and tactical grade MEMS gyroscopes are commercially available with a variety of packaging types and interface options. The measurement grade devices are targeted primarily at large volume applications such as automotive and motion/orientation sensing markets. Since the volume is high the cost per device can be low, but the ability to specialize the package and interface is limited without significant additional cost. The tactical navigation gyroscope applications are targeted mainly for a smaller military market, thus the cost can be significantly higher. Table 3 is an attempt to summarize companies who can supply these COTS parts.

Table 3. COTS MEMS Gyroscope Grade and Suppliers.

Sensor Technology	Sensitivity (Bias Stability)	Power	Cost	Supplier	Product Series
Measurement Grade	>100 °/hr	30-100 mW	~ $30 to several $100 ea	www.analog.com	ADXRS
				www.siliconsensing.com	CRS
				www.systron.com	QRS
				www.semiconductors.bosch.de	SMG
				www.xbow.com	VG
				www.memsense.com	
Tactical Grade	1 – 10 °/hr	~500 mW	~$5K/ea	www.honeywell.com	HG
				www.siliconsensing.com	SiRRS
				www.systron.com	SDG

3.3 Gravity Gradiometer

A gravity gradiometer is a unique though largely unfamiliar instrument that has a long history of development and a number of very valuable uses. The Scientific American article [36] by R. E. Bell gives a very good overview of the history and application of a gravity gradiometers.

The phenomena of gravity can be described starting with the Gravitational potential,Φ, which is a scalar or a zero order tensor:

13) $$\Phi = \frac{C}{r} = \frac{\Gamma M m}{r}$$

where,

Γ - Gravitation Constant [6.67×10^{-11} $(N\text{-}M^2)/Kg^2$]

M, m - Masses

r - Distance vector between M and m

The gravity force, G, is the gradient of the potential, Φ. The gravity force, **G**, is a vector or 1st order tensor, which describes the force in the three dimensions of space.

14) $$\boldsymbol{G} = \nabla\Phi = \frac{\partial\Phi}{\partial x}\vec{i} + \frac{\partial\Phi}{\partial y}\vec{j} + \frac{\partial\Phi}{\partial z}\vec{k} = G_x + G_y + G_z$$

Where gravity is a three dimensional vector, the gravity gradient is a 2nd order tensor which requires nine separate quantities to fully define. The gravity gradient is a second order tensor (i.e. matrix) which is defined as the *gradient* of the gravity force. The gravity gradient at a given position is described by the nine quantities of the second order tensor. However, since the gravity field is described by a Laplace partial differential equation (i.e. $G_{xx}+G_{yy}+G_{zz}=0$) and the matrix is symmetric and only five of the nine quantities are independent. These quantities can be arranged to in a square matrix notation.

15) $$\nabla G = \begin{bmatrix} G_{xx} & G_{yx} & G_{zx} \\ G_{xy} & G_{yy} & G_{zy} \\ G_{xz} & G_{yz} & G_{zz} \end{bmatrix} = \begin{bmatrix} G_{xx} & G_{yx} & G_{zx} \\ G_{yx} & G_{yy} & G_{zy} \\ G_{zx} & G_{zy} & G_{zz} \end{bmatrix}$$

The gravimeters (i.e. instruments which measure gravity) are a measure of gravity at one position; however, the *gravity gradient describes how gravity is changing with position at that position*. And, unlike optical or electro-magnetic environments, *gravity gradients can not be hidden or screened from observation*. For these reasons *gravity gradients are more descriptive of changes in the gravitational field due to anomalies such as subsurface mineral deposits or voids* [36,37], large massive objects such as submerged mountains to alert submarine commanders for dangers or for navigation aids [38]. Gravity gradiometers have also been used for port security screening [39,40].

A gravity gradiometer is an incredibly sensitive device that will measure the derivative of gravity with respect to distance. The unit of measure for the gravity gradient is the Eotvos (10^{-9} s^{-2}), which is approximately equal to the gradient of the gravitational force field produced by 10 grains (~ 9 milligrams) of sand at a distance of 1 centimeter. Modern gravity gradiometers have a resolution of < 1 eotvos.

The initial instruments developed to measure the gravity gradient were a torsion balance developed by Baron Roland von Eotvos in 1890, Figure 13. This type of instrument was used for geological and oil exploration in spite of its unwieldy and time consuming setup until the 1930's. In the 1960 with the advance in electronics and sensors such as accelerometers, work was initiated in the development of gravity gradient sensors [41]. Figure 14 is an example of an initial attempt of gravity gradient sensor development. With the mobility that the development of a sensor of this type provides the gradiometer has applicability in a number of areas, such as geophysical exploration, military applications such as submarine navigation. Modern embodiments of gravity gradiometers incorporate as many as 12 low noise, matched pendulous accelerometers (Bell aerospace model VII) to reject common mode signals arranged on rotating platforms in 3 axes at low frequency (e.g. 0.25 Hz). The rotation results in the gravity gradient signal being modulated at 0.5 Hz, while the common mode signal due to static gravity is at 0.25 Hz, providing a further ability for common mode rejection.

Examples of existing commercial applications are Lockheed Martin [42] for Military application, and BPH Brillion [43], which has developed the Falcon™ airborne gravity gradiometer system for geophysical exploration.

Research is under way at NASA, Jet Propulsion Laboratory to develop a Space flyable atomic interferometer based gravity gradiometer, [44].

Figure 13. Early torsion balance Gradiometer developed by Baron Roland von Eotvos in 1890.

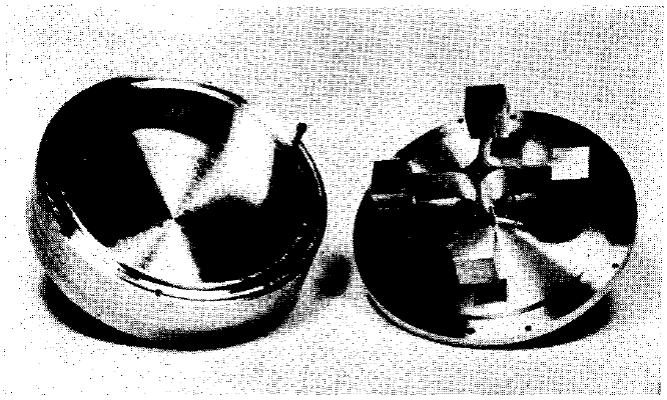

Figure 14. Five inch diameter Cruciform gravitational mass sensor using piezoelectric transduction, [41].

3. SUMMARY

This report reviews the field of MEMS inertial sensors. MEMS inertial sensors have made tremendous impact in the commercial world of motion sensing, and in automotive applications. There are COTS MEMS measurement and tactical grade inertial sensors. The entry of MEMS sensors into the navigation grade arena is being pushed by research programs funded by Sandia National Laboratories and government agencies such as DARPA, and ONR.

The type of transduction methods are described as well as the type of inertial sensors themselves. The transduction methods that are discussed include capacitative, piezoresistive, optical, electron tunneling, atomic interferometer and nuclear magnetic resonance. Capacitative and piezoelectric are the most prevalent in COTS MEMS inertial sensor. The other methods are currently in R&D to attempt to produce a navigation grade MEMS inertial sensor.

The history and method of inertial sensor operation are also discussed. The accelerometer, gyroscope and gravity gradiometer are the type of inertial sensors which are reviewed in this report. Their method of operation and a sampling of COTS sensors and grade are reviewed as well. The complexity involved in their design increases significantly from the accelerometer to the gyroscope to the gravity gradiometer which is the most complex. The type of application of each of these sensors is also discussed.

4. REFERENCES

1. G. Binning, H. Rohrer, Scanning Tunneling Microscopy, *IBM J. Res. Develop.*, 30, 355, 1986.
2. T. W. Kenny, W. J. Kaiser, S. B. Waltman, J. K. Reynolds. Novel infrared detector based on a tunneling displacement transducer, Appl. Phys. Lett. 59(15), 7 October 1991.
3. D. DiLella, L. J. Whitman, J. J. Colton, T. W. Kenny, W. J. Kaiser, E. C. Vote, J. A. Podosek, L. M. Miller. A micromachined magnetic-field sensor based on an electron tunneling displacement transducer, Sensors and Actuators 86, pp. 8-20, 2000.
4. T. W. Kenny, W. J. Kaiser, J. K. Reynolds, J. A. Podosek, H. K. Rockstand, E. C. Vote, and S. B. Waltman. Electron tunnel sensors, J. Vac. Sci. Technol. A 10(4), Jul/Aug 1992.
5. C. H. Liu and T. W. Kenny, "A high-precision, wide-bandwidth micromachined tunneling accelerometer," J. Microelectromech. Syst., vol. 10, no. 3, pp. 425-433, Sep. 2001.
6. R. L. Waters, M. E. Aklufi, T. E. Jones, "Electro-optical ultra sensitive accelerometer," IEEE Position Location and Navigation Symposium, pp. 36-43, 2002.
7. N. C. Loh, M. A. Schmidt, S. R. Manalis, "Sub-10 cm3 interferometric accelerometer with nano-g resolution," J. Microelectromech, Syst., vol. 11, no. 3, pp. 182-187, Jun. 2002.
8. B.E.N. Keeler, et. al., "Experimental demonstration of a laterally deformable optical nanoelectromechanical system grating transducer," Optics Letters, Vol. 29, Issue 11, pp. 1182-1184, 2004.
9. N. A. Hall, R. Littrell, M. Okandan, B. Bicen, and F. L. Degertekin, "Micromachined optical microphones with low thermal-mechanical noise Levels," JASA, V
10. N. A. Hall, et. al., "Micromachined Accelerometers with Optical Interferometric Read-Out, and Integrated Electrostatic Actuation," JMEMS, Vol. 17, No. 1, Feb. 2008.
11. U. Krishnamoorthy, D. W. Carr, G. R. Bogart, M. S. Baker, R. H. Olsson, "In-plane nano-G accelerometer based on an optical resonant detection system," Transducers '07, pp. 1195-1198, 2007.
12. U. Krishnamoorthy, et al., "In-plane MEMS-based nano-g accelerometer with sub-wavelength optical resonant sensor," Sensors and Actuators A, Vol, 145-146, pp. 283-290, July-August 2008.
13. M. Kasevich, S. Chu, "Measurement of the gravitational acceleration of an atom with a light –pulsed atom interferometer," Appl. Phys. B 54, 321, 1992.
14. B. C. Grover, U. S. Patent 4,430,616, Issued February 7, 1984
15. W. T. Thomson, Theory of Vibration with Applications, Prentice Hall, Inc., Englewood Cliffs, NJ, 1981.
16. C. Shearwood, C. B. Williams, P. H. Mellor, R. B. Yates, M. R. J. Gibbs, A. D. Mattingley, Levitation of a micromachined rotor for application in a rotating gyroscope, Electron. Lett. Vol. 31, No. 21, pp. 1845-1846, 1995.
17. C. Shearwood, K. Y. Ho, C. B. Williams, H. Gong, Development of a levitated micromotor for application as a gyroscope, Sensors and Actuators, Vol. 83, pp. 85-92, 2000.
18. Archangel Systems Inc., www.archangel.com
19. G. Sagnac, C. R. Acad. Sci., Vol. 95, pp. 707-710 and pp. 1410-1413, 1913.
20. A. Lawrence, Modern Inertial Technology, Springer 1998.
21. A. W. Lawrence, Thin film laser gyro, U. S. Patent 4,326,803, issued 27 April 1982.
22. C. Monovoukas, A. K. Swiecki, F. Maseeh, Integrated optical gyroscopes offering low cost, small size and vibration immunity, Proc. SPIE, Vol. 3936, pp. 293-300, 2000.
23. G. A. Vawter, et. al., Developments in Pursuit of a Micro-Optic Gyroscope, Sandia Report SAND2003_0665, 2003.
24. J. Lyman, E. Norden, Rate and attitude indicating instrument, U. S. Patent 2,309,853, issued Apr. 10, 1941.
25. J. Lyman, Angular velocity responsive apparatus, U. S. Patent, 2,513, 340, issued Oct. 17, 1945.
26. W. H. Quick, Theory of the vibrating string as an angular motion sensor, Trans. ASME, J. Appl. Mech., pp. 523-534, Sept. 1964.
27. D. Boocock, L. Maunder, Vibration of a symmetric tuning fork, J. Mech. Eng. Sci., Vol. 11, No. 4, 1969.
28. G. W. Hunt, A. E. W. Hobbs, Development of an accurate tuning-fork gyroscope, Symposium on Gryos, Proc. Inst. Mech. Eng., Vol. 179, No. 3E., 1964-1965.
29. W. P. Chan, F. Prete, M. H. Dickinson, Visual input to the efferent control of a fly's gyroscope, Science, Vol. 280, No. 5361, pp. 289-292, April 10, 1998.
30. W. A. Clark, Micromachined Vibratory Rate Gyroscopes, Ph.D. Dissertation, University of California, Berkeley, Fall 1997.
31. W. A. Clark, R. T. Howe, R. Horowitz, Surface micromachined Z-axis vibratory rate gyroscope, Technical Digest Solid-State Sensor and Actuator Workshop, pp.283-287, June 1996
32. J. M. O'Connor, D. M.Shupe, Vibrating Beam rotation sensor, U. S. Patent 4,381,672, issued May 3, 1983.

33. B. Greiff, T. Boxenhorn, T. King, L. Niles, Silicon Monolithic Gyroscope, Transducers '91, Digest of Technical Papers, pp. 966-969, 1991.
34. A. Kourepenis, J. Borenstein, J. Connelly, R. Elliott, P. Ward, M. Weinberg, IEEE 1998 Position Location and Navigation Symposium, PLANS 98, pp. 1-8, 1998.
35. J. A. Green, S. J. Silverman, J. F. Chang, S. R. Lewis, Single-Chip Surface Micromachined Integrated Gyroscope with 50°/h Allan Deviation, IEEE J. of Solid-State Circuits, Vol. 37, No. 12, Dec. 2002.
36. R. E. Bell, Gravity Gradiometry, Scientific American, June 1998, pp. 74/
37. A. H. Streland, Going Deep: A System Concept for Detecting Deeply Buried Facilities from Space, Air War College report, Feb. 2003.
38. J. Moryl, Advance Submarine Navigation Systems, Sea Technology, Nov. 1996, pp. 33-39.
39. B. Kirkendall, Y. Li, D. Oldenburg, Imaging cargo containers using gravity gradiometry, Proc. of SPIE, Vol. 6204.
40. J. Parmentola, The Gravity Gradiometer as a Verification Tool, Science & Global Security, Vol. 2, pp. 43-57, 1990.
41. C. C. Bell, et. al., Vibrational Mode Behavior of Rotating Cruciform Gravitational Gradient Sensors, Journal of Applied Physics, Vol. 39, Num. 7, June 1968.
42. D. DiFrancesco, Gravity Gradiometery Developments at Lockheed Martin, Geophysical Research Abstracts, Vol. 5, 01069, 2003.
43. BHP Billiton: www.bhpbilliton.com
44. N. Yu, et. al., Development of an atom-interferometer gravity gradiometer for gravity measurement from space, Applied Physics B, Vol. 84, issue 4, p. 647-652, Sept. 2006.

DISTRIBUTION

1	MS1185	D. L. Davidson	5417
1	MS1080	K. Ortiz	1749
1	MS0783	J. J. Allen	6473
1	MS1003	G. V. Sanzero	6473
1	MS0899	Technical Library (electronic copy)	9536


Sandia National Laboratories